LBNL-47032

ERNEST ORLANDO LAWRENCE
BERKELEY NATIONAL LABORATORY

Seismic Mapping of the Subsurface Structure at the Ryepatch Geothermal Reservoir

Roland Gritto, Thomas M. Daley,
and Ernest L. Majer

Earth Sciences Division

October 2000

DISCLAIMER

LBNL-47032

Seismic Mapping of the Subsurface Structure at the Ryepatch Geothermal Reservoir

Roland Gritto, Thomas M. Daley, and Ernest L. Majer

Earth Sciences Division, Lawrence Berkeley National Laboratory, Berkeley, California

October 2000

This research was supported by the Assistant Secretary for Energy Efficiency and Renewable Energy, Office of Geothermal and Wind Technologies of the US Department of Energy under contract No. DE-AC0376SF00098. Computations were carried out at the Center for Computational Seismology of the Lawrence Berkeley National Laboratory.

Seismic Mapping of the Subsurface Structure at the Ryepatch Geothermal Reservoir

Roland Gritto, Thomas M. Daley, and Ernest L. Majer

Earth Sciences Division, Lawrence Berkeley National Laboratory, Berkeley, CA

Abstract

In 1998 a 3-D surface seismic survey was conducted to explore the structure of the Rye Patch geothermal reservoir (Nevada) to determine if modern seismic techniques could be successfully applied in geothermal environments. Furthermore, it was intended to map the structural features which may control geothermal production in the reservoir. The results suggested the presence of at least one dominant fault responsible for the migration of fluids in the reservoir. In addition to the surface receivers, a 3-component seismometer was deployed in a borehole at a depth of 3900 ft within the basement below the reservoir, which recorded the waves generated by all surface sources. The subject of this report is use this data set to determine the subsurface structure as a function of azimuth. A total or 2005 first arrival travel times were determined out of 2134 possible traces. 2-D ray tracing was performed to simulate wave propagation from the surface sources to the receiver at depth. The ray tracing was based on a 2-D laterally homogeneous velocity model derived from a velocity profile calculated from a VSP recorded in the same well. It was assumed that differences in travel time between the observed and modeled data are caused by structural deviations from a homogeneously layered model as determined by the VSP profile, and thus were mapped into topographic changes at depth. The results suggest an east-west-trending structure (possibly a horst) with boundaries that match the location of faults found in the analysis of the 3-D seismic surface data.

1. Introduction

In recent years Lawrence Berkeley National Laboratory (LBNL) has been cooperating with The Industrial Corporation (TIC) and Transpacific Geothermal Inc. (TGI) to evaluate and apply modern seismic imaging methods for geothermal reservoir definition under the U.S. Department of Energy's (DOE) geothermal program. As part of this cooperation a vertical seismic profile (VSP) was acquired in 1997 and a 3-D seismic survey was performed in 1998 at the Rye Patch Geothermal field in Nevada, to determine the structure of the subsurface reservoir. The VSP survey was conducted to determine the seismic reflectivity of the reservoir horizons and to obtain reservoir velocity information. Because the results of the initial VSP profile indicated apparent reflections at depth *Feighner et al.* [1998], it was decided to proceed with the 3-D seismic survey to evaluate the application of modern seismic imaging techniques to geothermal reservoirs.

Geothermal reservoirs are considered difficult seismic targets because of hydrothermal alteration and other heterogeneity. As part of the 3-D seismic surface survey, an additional experiment was conducted during which a 3-component geophone was installed at a depth of 3900 ft. This geophone recorded all seismic waves generated by the surface sources, creating a second dataset in addition to the seismic reflection data. The investigation of the second dataset is the content of this report.

The location of the surface survey and the location of borehole 46-28 containing the geophone at depth are indicated in Figure 1 (modified after *GeothermEx* [1997]). The Rye Patch temperature anomaly is bounded by the Humbold City Thrust in the East and the Rye Patch reservoir in the West. Initial geothermal exploration efforts in the 1980s and 1990s resulted in one successful well (44-28) while others were too cold or had no fluid flow. The 3-D seismic survey was intended to determine the applicability of modern seismic imaging techniques to geothermal reservoirs and in particular to study the geologic structure of the reservoir at depth. An initial report by *Feighner et al.* [1999] revealed possible faulting at depth based on results derived from surface reflection seismic studies and surface-to-surface tomographic travel time investigations. The current investigation is intended to determine whether the dataset, which was recorded with minimal extra effort at depth, can provide additional valuable information and if so, whether it can support the results found in the previous studies.

2. Data Acquisition and Processing

The Rye Patch Geothermal Survey covered an area of 3.03 square miles and was designed with 12 north-south receiver lines and 25 east-west source lines. The source interval was 100 feet while the source line spacing was 400 feet. Four Litton 311 vibrators were used in a squared array with the source flag at the center of the array. The source signal was a sweep with a frequency bandwidth between 8 Hz and 60 Hz. A detailed description of the data collection can be found in the contractor's report *SECO* [1998].

A high temperature, wall-locking, 3-component geophone was installed in well 46-28 at a depth of 3900 ft. The borehole geophone recorded all shots throughout the survey area, amounting to a total of 2134 traces. The location of all sources as well as the boreholes are shown in Figure 2. The gaps in coverage are caused by Interstate 80 and railroad tracks which cross through the survey area.

The data quality is good with a frequency content of about 25 Hz for the first arriving waves. Figure 3 shows a representative receiver gather of source line

north of well 46-28. It is evident, as a first order effect, that the amplitudes and the moveout of the first arriving waves vary with distance to the well. Additionally, local and smaller variations in arrival time can be seen between source positions 10048 and 10063. These local variations in travel time will be mapped into topographic changes of the reservoir horizons at depth.

A total of 2001 first arrival travel times were determined out of 2134 possible traces. Most of the picks were reliable because the well sampled spatial moveout across the source lines facilitated the picking. However, in addition to the long source lines, "make-up lines" of 5 source locations were set up in between the original lines. The first arrival picking was less reliable for these shorter lines.

3. Ray Tracing

In 1997, a Vertical Seismic Profile (VSP) was recorded at the Ryepatch Geothermal field in well 46-28 *Feighner et al.* [1998]. The resulting P-wave velocity profile between the depth of 400 ft and 4150 ft represents the best estimate for the distribution of velocities in the subsurface around the well, and is the only in situ velocity measurement available. Based on these results, a velocity function was derived that represents a smoothed average of the VSP velocity profile. The function is shown in Figure 4. The prominent features of this velocity function are the high velocity layer of 11,500 ft/s between 700 ft and 800 ft depth, followed by a velocity inversion to approximately 9000 ft/s over a depth range of 1500 ft, and a gradual increase to 20,000 ft/s representing the basement at a depth of 2900 ft.

This velocity profile was subsequently extended to a 2-D velocity model with homogeneous layers extending throughout the survey area. Based on this velocity model, a 2-D ray tracer was used to simulate wave propagation from surface sources to the receiver at depth. Figure 5 shows representative results of the ray tracing. The velocity model is the 2-D representation of the function in Figure 4. Sources are denoted by stars while the receiver is indicated by an inverted triangle at 3900 ft depth. Figure 5a represents the rays for source line 20 which runs across well 46-28 from West to East, while Figure 5b shows the line between sources 1048 and 25048 running across the well in North-South direction. The gaps in source coverage indicate the railroad tracks, interstate 80, and an area in the vicinity of the well where no sources were fired. The top of the velocity model was chosen to be equal to the elevation of the highest source position of the survey, so the sources in the figure appear to be located below the surface.

The 2-D raytracing produced a total of 2134 rays, connecting the sources to the receiver at depth, and their associated travel times. None of the 2134 rays crossed path with other rays which prevented the application of a tomographic inversion approach. Therefore, we cannot simultaneously find lateral velocity variations within the layers. However, under the assumption that the homogeneous velocity model is a good representation of the subsurface structure (i.e. velocities can be extrapolated away from the borehole) the observed and modeled travel times can be compared for each source-receiver combination, and differences can be attributed to changes in elevation of the subsurface horizons.

4. Mapping Travel Time Deviations to Elevation Changes at Depth

4.1. Methodology

Mapping travel time deviations to elevation changes is a technique that has been used in seismic refrac-

tion studies in the past. The method is an approximation that can be applied in environments where a low velocity layer is located above a high velocity layer or basement. Under the assumption that the ray path from source to receiver is known, any difference between the calculated and observed travel times is converted into a distance using the velocity model and applied as a deviation in the boundary between the basement and the overlaying layer. We employ the same principle in our approach assuming that the top layer can be approximated by an average velocity of 9000 ft/s (refer to Figure 4), and the basement is represented by a halfspace with a velocity of 20,000 ft/s. The travel time deviations are computed for each ray path and the differences converted to elevation changes. In our case, we apply the total travel time difference for each ray to all of the layered sequence above the basement, thus assuming that any possible faulting affected the whole geologic sequence above the basement. However, this is only one possible interpretation of the data and other scenarios may be as likely. It is feasible that a fault cuts only through the basement and a fraction of the layers above, while in another case it may cut through the basement only. These later cases would represent events where sedimentation continued after the fault stopped being active. One of these later cases may be present at Ryepatch, where there is no surface evidence of the SE fault. However, as it is not possible to determine where the fault stops, we choose to interpret the whole sequence above the basement as being affected by tectonic activity.

Figure 6 shows the results of the differences in travel time δt between the calculated t_m and observed travel times t_o plotted for each source location.

$$\delta t = t_m - t_o \tag{1}$$

Positive deviations denote source positions from which the actual waves travel faster to the receiver than in the ray tracing simulations. The assumed explanation in this case is that the high velocity basement is uplifted relative to the homogeneously layered velocity model used in the simulations (refer to Figure 5). Similarly, negative deviations denote slower wave propagation than assumed in the simulations, indicating a thicker low velocity layer on top of the basement (e.g. the basement is shifted downwards).

4.2. Source Elevation Statics

Assuming the above interpretation is correct, the time-difference plot in Figure 6 would be a representation of the basement interface at depth. However, it is evident that the trend of the travel time deviations in Figure 6 also mimics the elevation of the sources throughout the survey area. Figure 7a shows a contour map of the source locations, while Figure 7b shows the same data in a 3-D view. The elevation of the sources decreases towards the West following the dip of the surface from the Humboldt City Thrust in the East to the Rye Patch Reservoir in the West (refer to Figure 1). The problem that occurs by using correct source locations with large elevation changes while applying a constant velocity model for the near surface layer that geologic processes often compensate for the shortcomings of this model. While the travel distance from sources at high elevation to the receiver at depth is longer, these source sites are usually exposed to stronger erosion which removes the low velocity sedimentary layers, and thus bedrock with higher velocities may be exposed to compensate for the longer travel distance. If, during the simulations, sources are placed at the correct elevations in conjunction with the use of a low velocity surface layer, the travel times of the simulations may become too long relative to the observed travel times and higher

travel time deviations are observed. The reverse effect may take place for lower elevations where thicker sedimentary fill may lower the velocities below the values of the assumed velocity model. Thus, a second simulation was performed to verify that the distribution of travel time differences in Figure 6 is not an artifact caused by the distribution of source locations during the survey. For this test all sources were located at a fixed elevation equal to the elevation at the well head of borehole 46-28. If the structure in Figure 6 was caused by static problems with the source locations, it would disappear or change after the simulations with a flat source-horizon. The same structure is present in both cases, as shown in Figure 8. Although the overall time differences decreased slightly relative to the results in Figure 6, the general feature of a high in the central eastern region of the survey area which decreases towards the West is still evident. Therefore, it is assumed that this feature is a real manifestation of a deviation from the assumed velocity model at depth. However, contrary to the eastern region of the survey area where the high in the center is bounded by small travel time deviations in the North and South, the western half of the survey reveals a pronounced trend to negative travel time deviations. These deviations are only partially reduced by the introduction of a flat source horizon in Figure 8. The reason for that may be very low sedimentary velocities on the western side of interstate 80 towards the Rye Patch Reservoir. In a previous study, *Feighner et al.* [1999] reported results from 2-D tomographic studies in North-South direction along the receiver lines at Rye Patch. Figure 9 shows the tomographic results along receiver line 1 located along the western boundary of the survey area. It can be seen that velocities as low as 5000 ft/s are estimated for the shallow subsurface down to depths of 200 ft. Because these velocities (if correctly estimated) are lower than the one assumed in our homogeneous model (6800 ft/s down to a depth of 700 ft, see Figure 4), the resulting travel time difference δt would be negative throughout this region. With these considerations in mind, the structure of the travel time deviations will be investigated more closely.

4.3. Interpretation

Figure 10 redisplays the travel time deviations from three different azimuths, in order to better recognize the structure. In Figure 10a (view from SW) the increase in travel time deviation is apparent in the background of the area but there's little evidence of an increase north and south of it. In the foreground of the image the large negative travel time deviations are evident, interrupted by smaller negative and even small positive values. Thus it seems that a structural feature is trending in an east-west direction, increasing the travel time deviations even in the western region of the survey area. These higher deviations could be explained by a lift of the high velocity basement relative to the overlaying structure. The views of Figure 10b and 10c support this interpretation. In Figure 10b (view from East) it is evident that the high terminates quickly to the North but shows a more gradual decrease toward the South. Similarly, in Figure 10c (view from West) the interruption of the low values in the foreground is abrupt to the North and more gradual to the South. Overall, the strike of this structure appears to be trending east-west.

After mapping the travel time deviations in Figure 8 to elevation differences using a basement velocity of 20,000 ft/s and a mean velocity of 9,000 ft/s for the section above the basement, the results are shown in Figure 11. The location of borehole 46-28 is shown for reference (black circle in foreground). The actual elevation changes of the basement horizon are probably smaller than the ones shown in the present map-

ping, since all deviations from the assumed horizontally layered velocity model are mapped into elevation changes. Additionally, this model may not be a good representation at great distances from the borehole, and it is feasible that a deviation in travel time is caused by a local velocity unconformity rather than a change in a boundary of the layered velocity model. However, it is not possible to estimate those local velocity changes with the present data, as this would constitute solution to a complex inversion problem for which data coverage with numerous crossing rays is needed. The current data set, however, does not contain any crossing rays in the subsurface. Thus, the estimated changes in elevation represent upper bounds for the actual values.

A mapview of the basement horizon elevation is provided in Figure 12. The three boreholes 46-28, 44-28, and 42-28 are shown for reference. It can be seen that the 0 ft elevation contour line runs through well 46-28, which is expected since the velocity model is based on the VSP data of well 46-28 and only a small deviation between the modeled and measured data is expected at this location. The map shows the contours of the elevated structure extending from East to West across the survey area while cutting through the steep descent on the western flank. The north-south extend of this rise reaches roughly from 2107000 (north of well 42-28) to 2102000 between wells 46-28 and 44-28 (refer to Figure 12).

4.4. Comparison to Previous Studies

A feature similar to the rise described above was detected in the study by *Feighner et al.* [1999], and is shown in Figure 13. The figure shows the velocity estimates from a tomography study along receiver line 13, at the eastern boundary of the survey area. Although the ray coverage was poor along most of the receiver lines, limiting the reliability of the tomographic results, the estimates in Figure 13 are based on good ray coverage within the upper 1500 feet. The depth penetration for the tomographic study is limited as the turning rays propagate from surface sources to surface receivers. The tomographic results reveal an elevated horizon of faster material in the center of the line between 2101000 and 2104000, which resembles the elevation high observed in the previous figures. Although the estimated location of the elevated section in Figure 12 and 13 is not the same, the match is acceptable considering that the result of Figure 12 is averaged over a large area, and Figure 13 represents a vertical depth slice. Thus it is possible that the elevation high in both Figures is a manifestation of the same geologic process. It should be noted that the elevated high velocity horizon seen at the margins of the image in Figure 13 is an artifact of the ray geometry and does not represent actual subsurface structure.

In 1999, an integrated study based on various geophysical data was conducted by Teplow Geologic (*Teplow* [1999]). This study included, among other results, the interpretation of the seismic reflection lines produced by *Feighner et al.* [1999]. Figures 14, 15, and 16 show, respectively, the reproduced results of the gravity, magnetic, and self potential data, that was collected over the Rye Patch geothermal area. The upper panels show the actual locations of the data measurement, while the lower panels reveal a contour map of the data values. Figure 14 shows the Bouguer gravity residual which indicates a broad region of constant values bounded by steep negative gravity gradients to the north-west and south-east. The results support the interpretation of higher density or excess mass in the central region around the wells, surrounded by less dense material (e.g. an elevated high density basement may represent a fitting model). Figure 15 shows the total magnetic field. The contour lines reveal an east-west trending feature

with a low in the central part between the boreholes. A possible explanation may be the presence of hydrothermal mineralization in the alluvial deposits of the area (*Teplow* [1999]). The self potential data (Figure 16) support the trend of the magnetic and gravity surveys. Again, the data reveal a low in east-west direction around well 44-28 bounded by gradients to the North and South.

Overall, it can be stated that the self potential, magnetic and gravity data presented above support the interpretation of an east-west feature in the central region around the boreholes and therefore corroborates the results of the seismic mapping in the present study.

5. Conclusions

The geophysical experiments conducted at Rye Patch geothermal field, provided various datasets which help to interpret the subsurface structure of the reservoir. The addition of a depth geophone to record surface generated seismic waves during the 3-D reflection survey provided an additional independent dataset at low cost and a minimum of technical and labor requirements. Because most geothermal areas provide access to open boreholes during the developing stages of the reservoir, it is recommended that a VSP survey is conducted first, to obtain information about the velocity structure and the reflectivity of the subsurface. These in situ measurements are the only direct method to determine seismic velocities at depth, and are imperative for the planing of any future surface seismic reflection surveys. VSP results are normally extrapolated from the vicinity of the borehole into the surrounding area to provide a 3-D velocity model. However, because of the heterogeneous nature of geothermal reservoirs, the error in extrapolating the VSP information can be minimized by conducting VSP surveys in multiple boreholes throughout the reservoir. A suite of VSP surveys is highly recommended for any reservoir exploration, since all following seismic experiments reply on the velocity information derived from these surveys. If it is determined that a surface seismic reflection survey may provide more detailed information about the reservoir structure it is recommended to add geophones in any available borehole within the survey area. These datasets collected at depth provide an independent, low-cost alternative to the surface data, and can help in the interpretation of the subsurface structure.

In the current study, the data recorded in borehole 46-28 provided information that supports results from previous experiments. The interpretation of an elevated basement with an east-west trend bounded by linear features towards the northern and southern extension is in agreement with 2-D tomographic results (*Feighner et al.* [1999]) and possibly with geophysical investigations undertaken in a previous study (*Teplow* [1999]). However, it should be recalled that the interpretation of an elevated basement is just one of several structural models that can explain the data. Furthermore, the uplift that is indicated in Figures 11 and 12, should be seen as an upper bound on the actual lift, as the total amount of the travel time difference between the observed and modeled travel times is converted to lift, rather than viewed as horizontal velocity variations, which are undoubtly present in the reservoir. In order to estimate the lateral velocity variations, however, a dataset is needed that contains multiple crossing raypaths, which are not present in the current data.

Acknowledgments. This work was supported by the Assistant Secretary for Energy Efficiency and Renewable Energy, Office of Geothermal and Wind

Technologies of the US Department of Energy under contract No. DE-AC03-76SF00098. All computation were carried out at the Center for Computational Seismology of the Lawrence Berkeley National Laboratory.

References

Feighner, M., Daley, T.M., Majer, E.L., 1998, Results of Vertical Seismic Profiling at Well 46-28, Rye Patch Geothermal Field, Pershing County, Nevada, *Lawrence Berkeley National Laboratory Report LBNL-41800.*

Feighner, M., Gritto, R., Daley, T.M., Keers, H., Majer, E.L., 1999, Three-Dimensional Seismic Imaging of the Ryepatch Geothermal Reservoir, *Lawrence Berkeley National Laboratory Report LBNL-44119.*

GeothermEx, 1997, Geology of the Rye Patch Geothermal Field, Pershing County, Nevada, *Internal Report, GeothermEx, Inc., Richmond, California.*

SECO, 1998, 3-D Seismic Survey, Rye Patch Geothermal Field, Pershing County, Nevada, June-August 1998, *Report, Subsurface Exploration Company, Pasadena, CA.*

Teplow, B., 1999, Integrated Geophysical Exploration Program at the Rye Patch Geothermal Field, Pershing County, Nevada - Final Report.

R. Gritto, T. M. Daley, E. L. Majer, Earth Sciences Division, Lawrence Berkeley National Laboratory, 1 Cyclotron Road, M.S. 90-1116, Berkeley, CA 94720 (rgritto@lbl.gov, tmdaley@lbl.gov, elmajer@lbl.gov)

This preprint was prepared with AGU's LaTeX macros v4. File report formatted October 31, 2000.

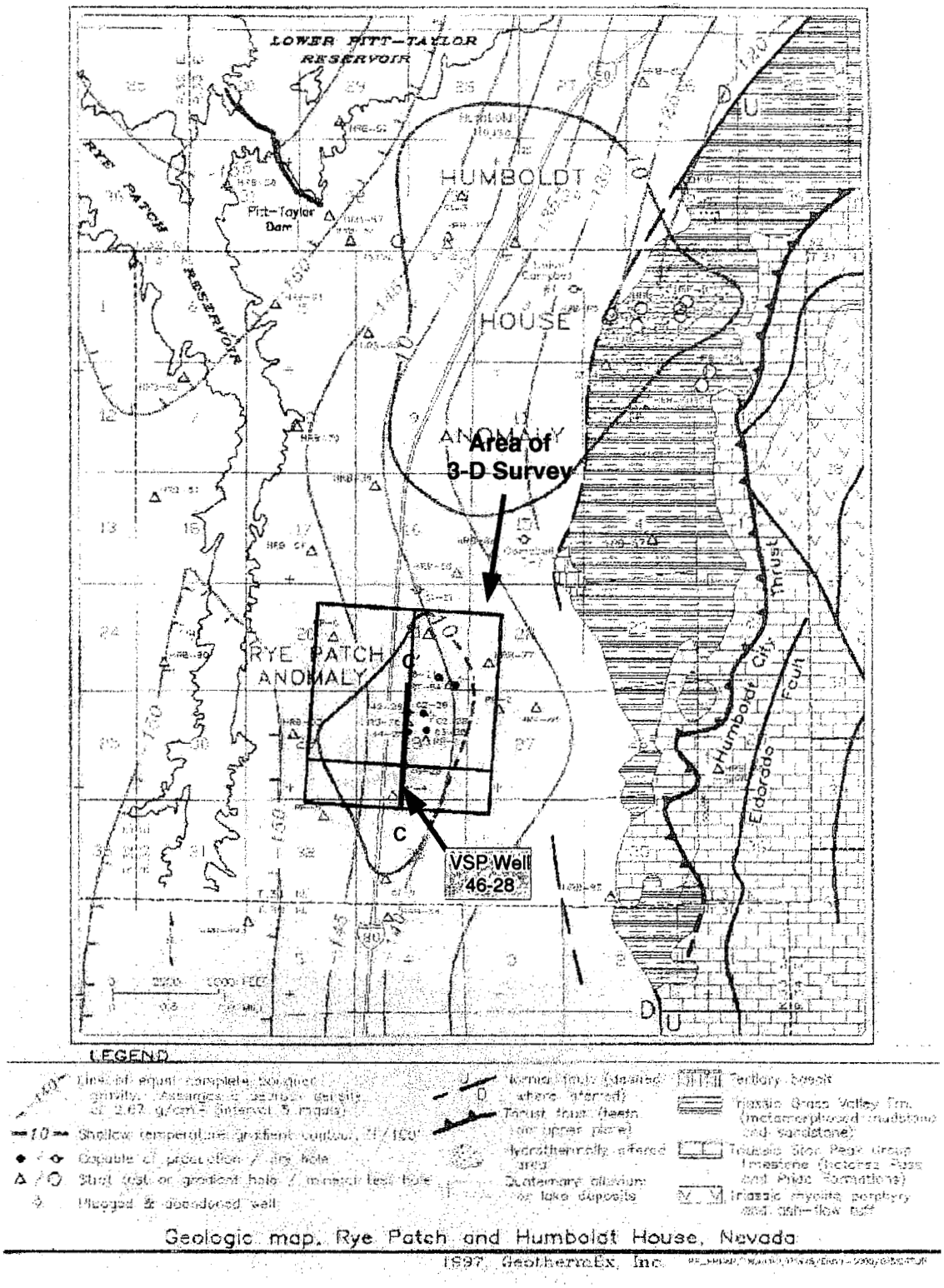

Figure 1. Location map with area of 3-D survey. The location of VSP Well 46-28 is indicated by the arrow.

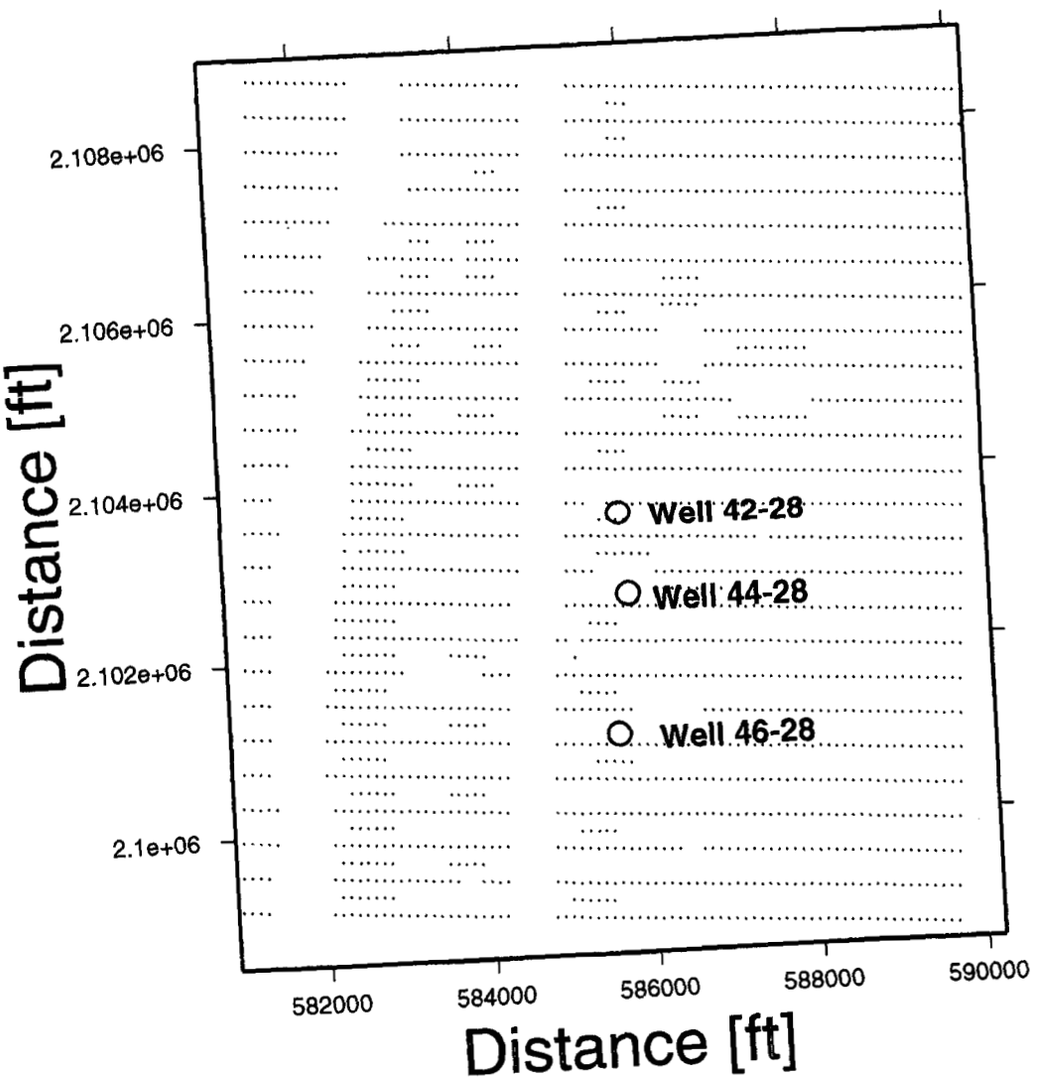

Figure 2. Map indicating the locations of the source points during the 3-D seismic surface survey and the location of wells 42-28, 44-28, and 46-28.

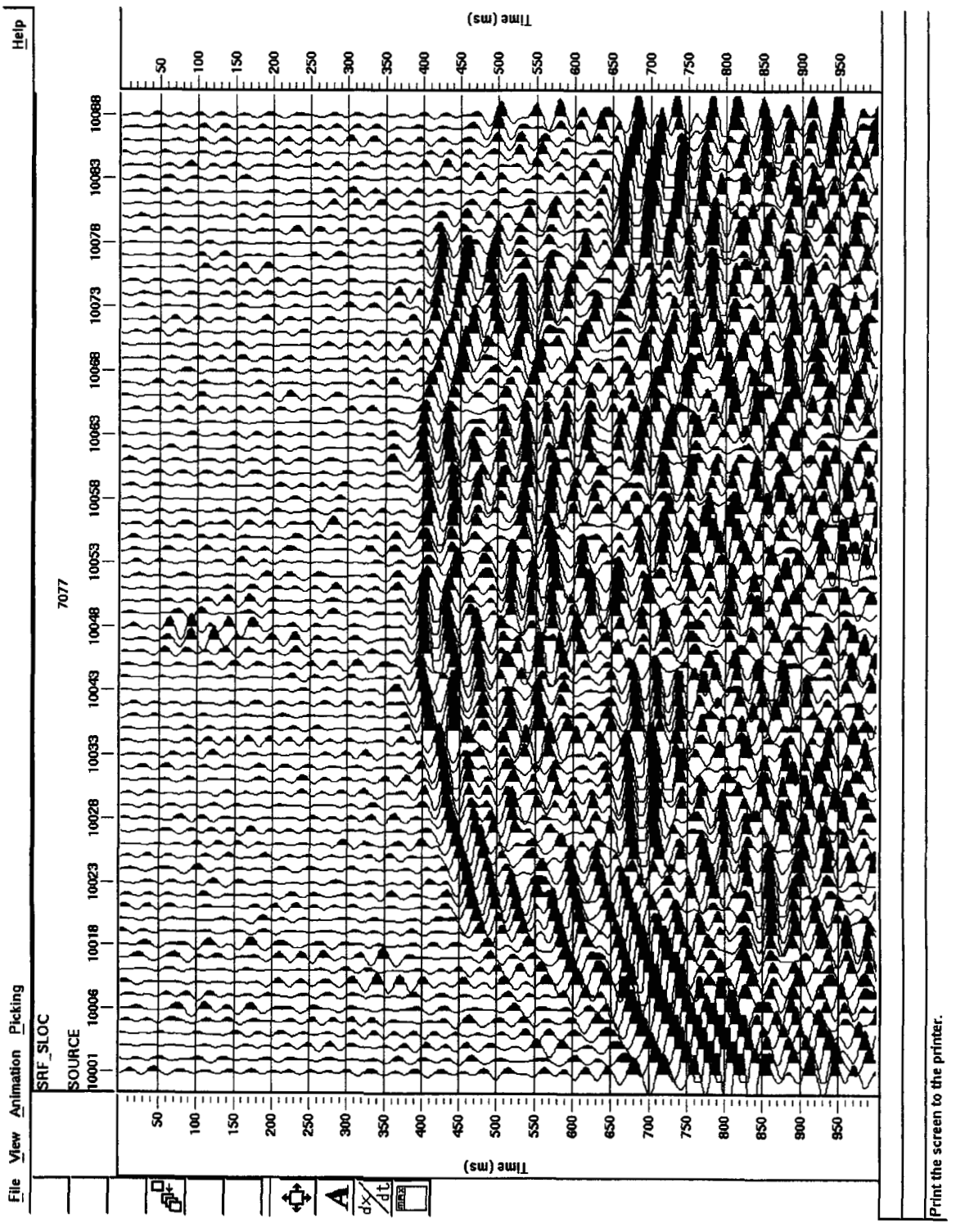

Figure 3. Common receiver gather for all sources in source line 10.

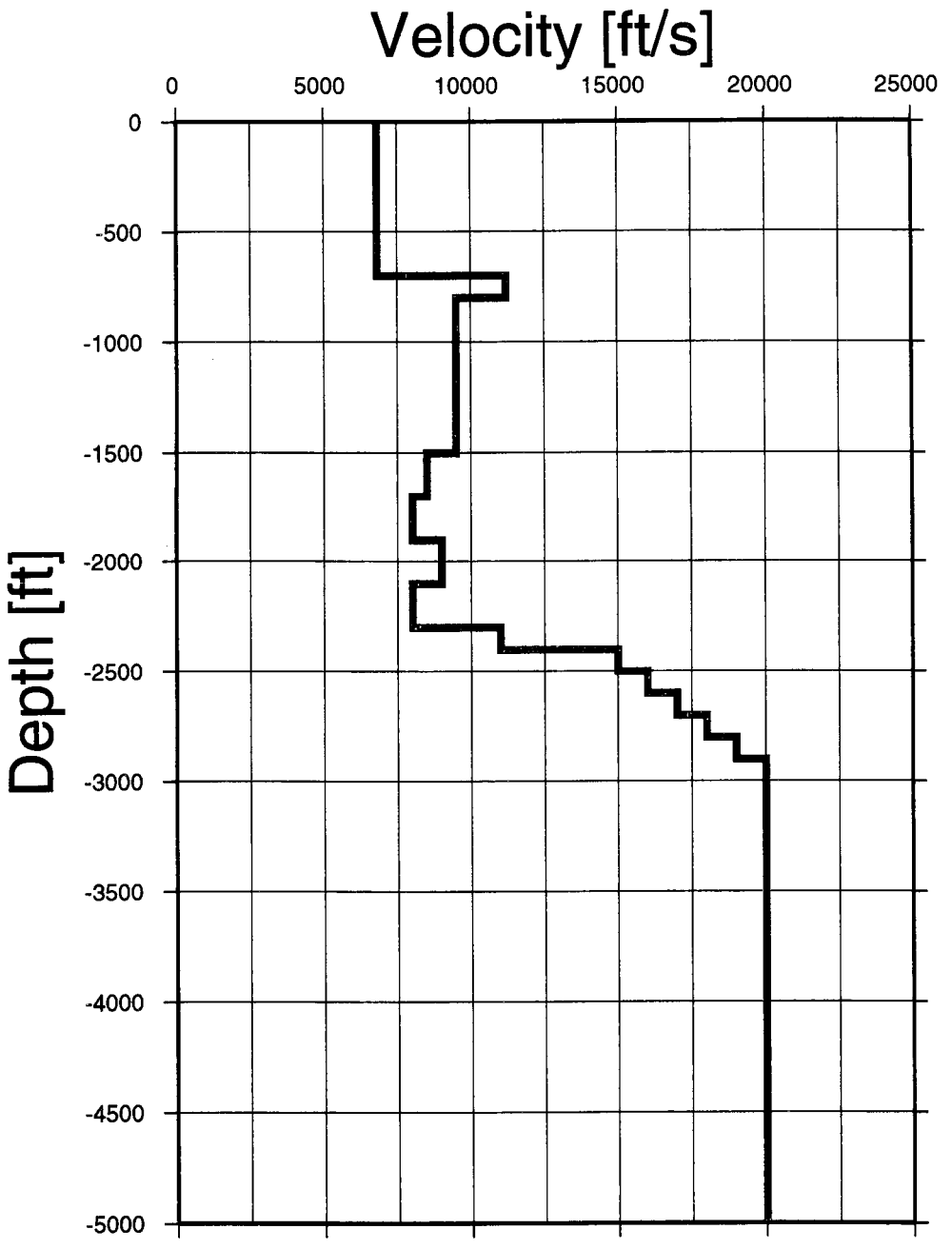

Figure 4. Velocity profile from the VSP survey in Well 46-28.

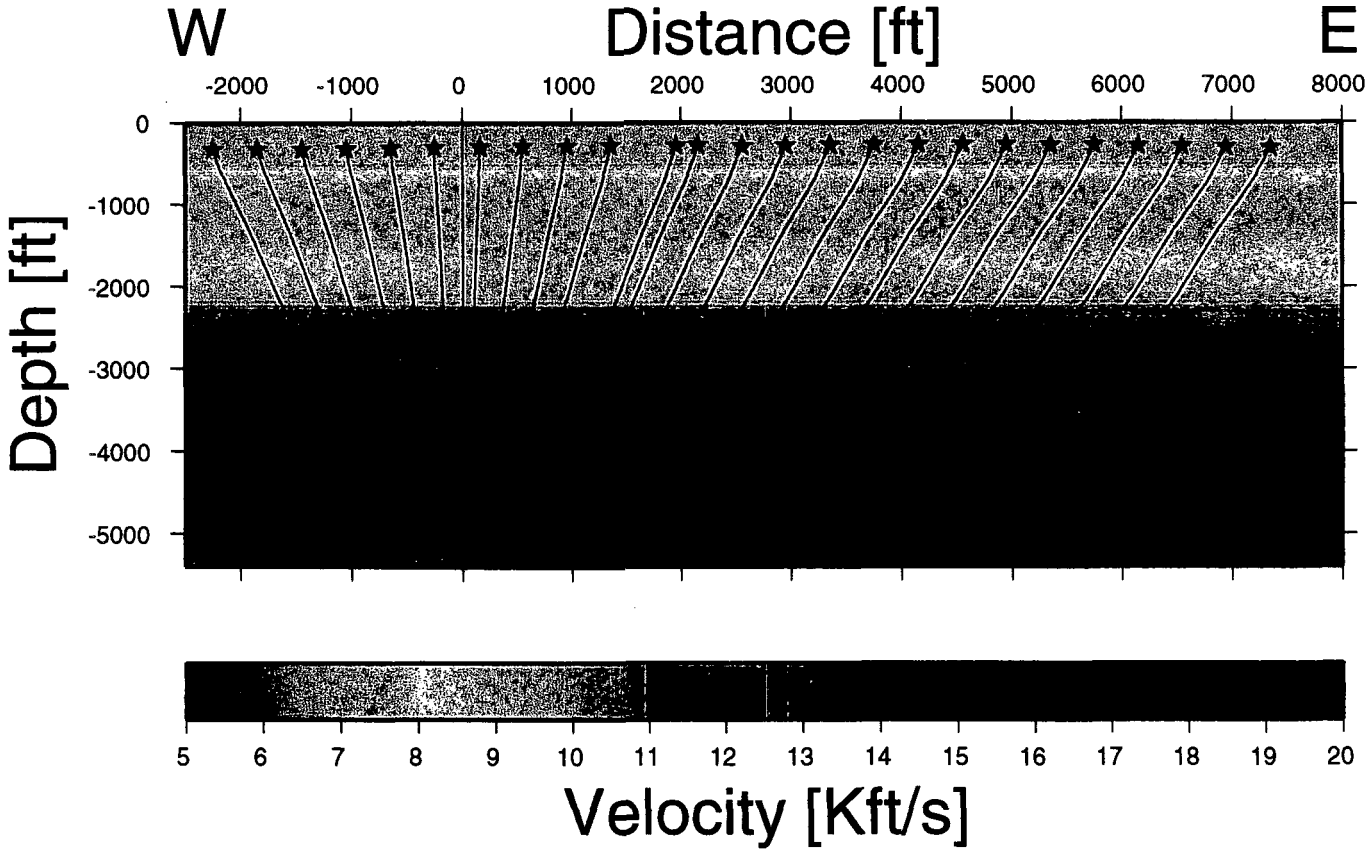

Figure 5a. Velocity model and ray paths from the sources in source line 20 to the receiver in well 46-28.

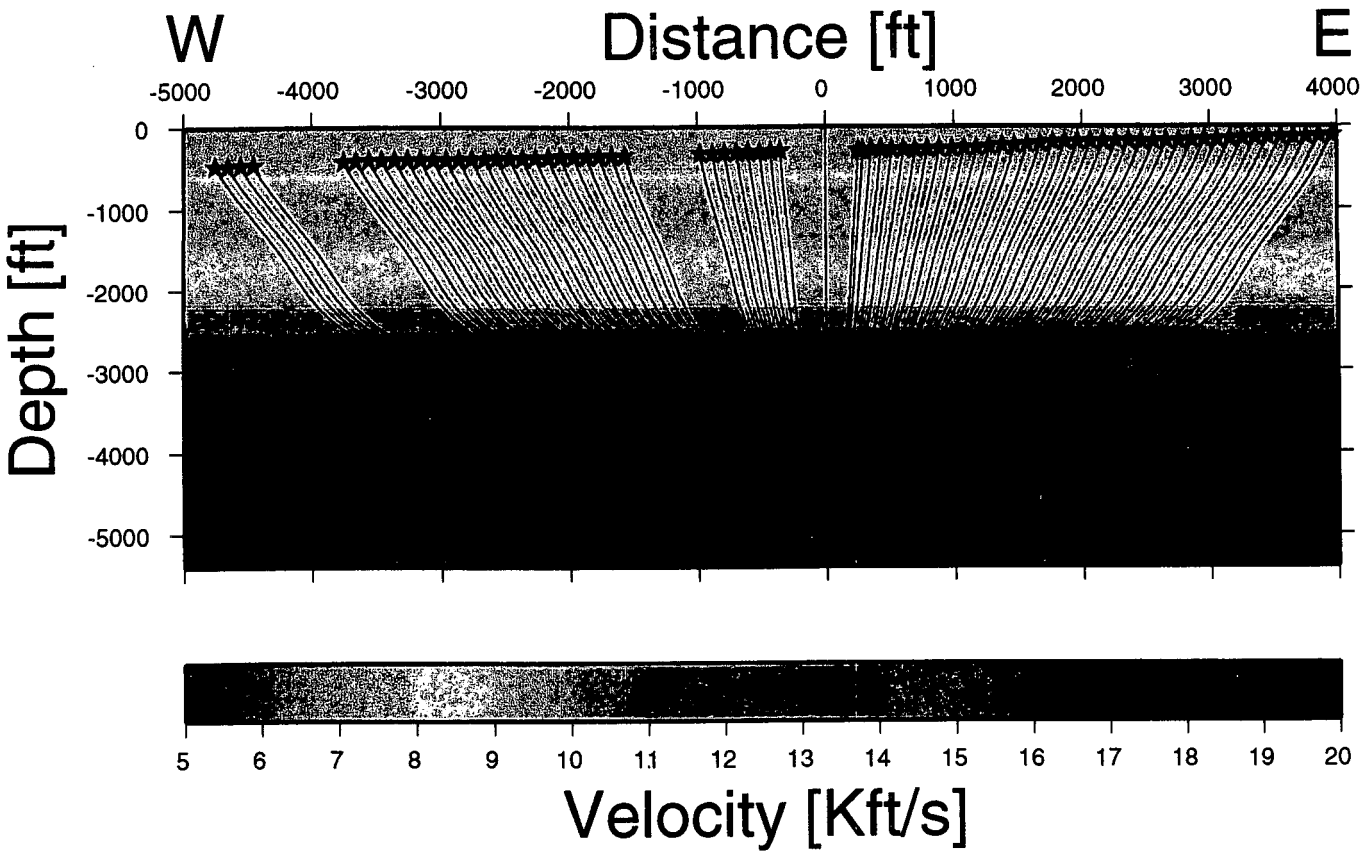

Figure 5b. Velocity model and ray paths from source numbers 1048 to 25048 to the receiver in well 46-28.

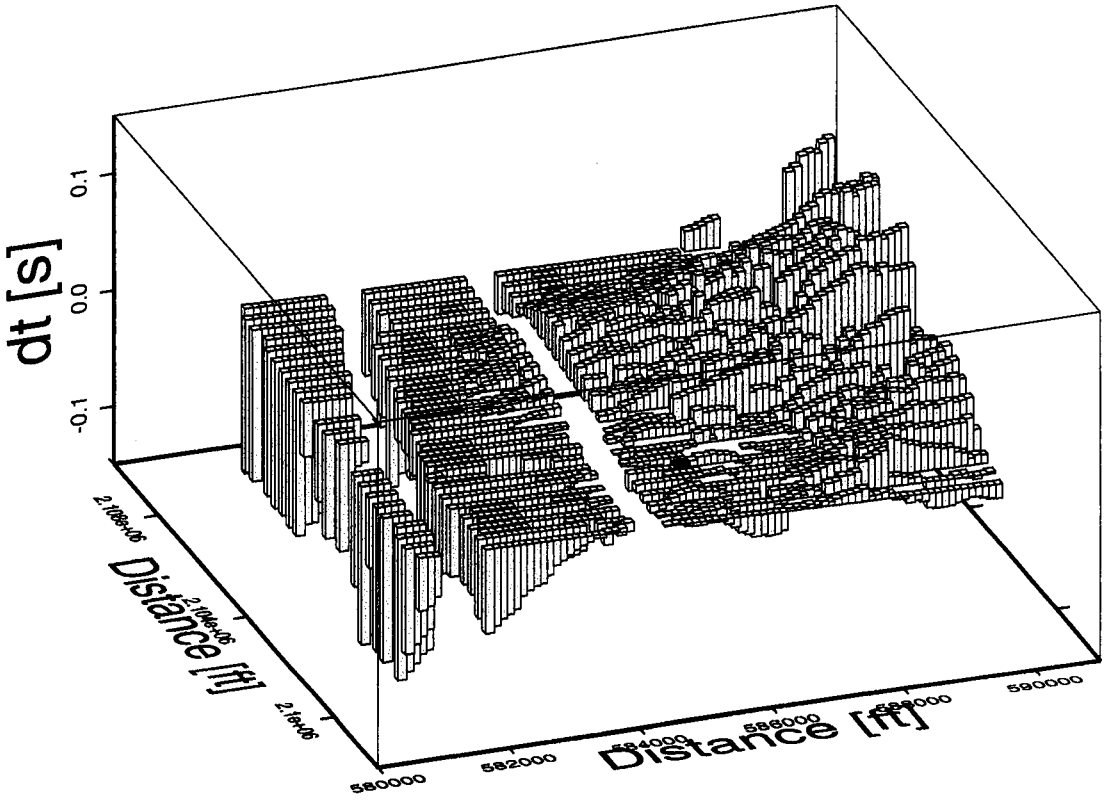

Figure 6. Travel time differences between the observed and modeled travel times. VSP well 46-28 is indicated by the circle in the foreground. View from South-West.

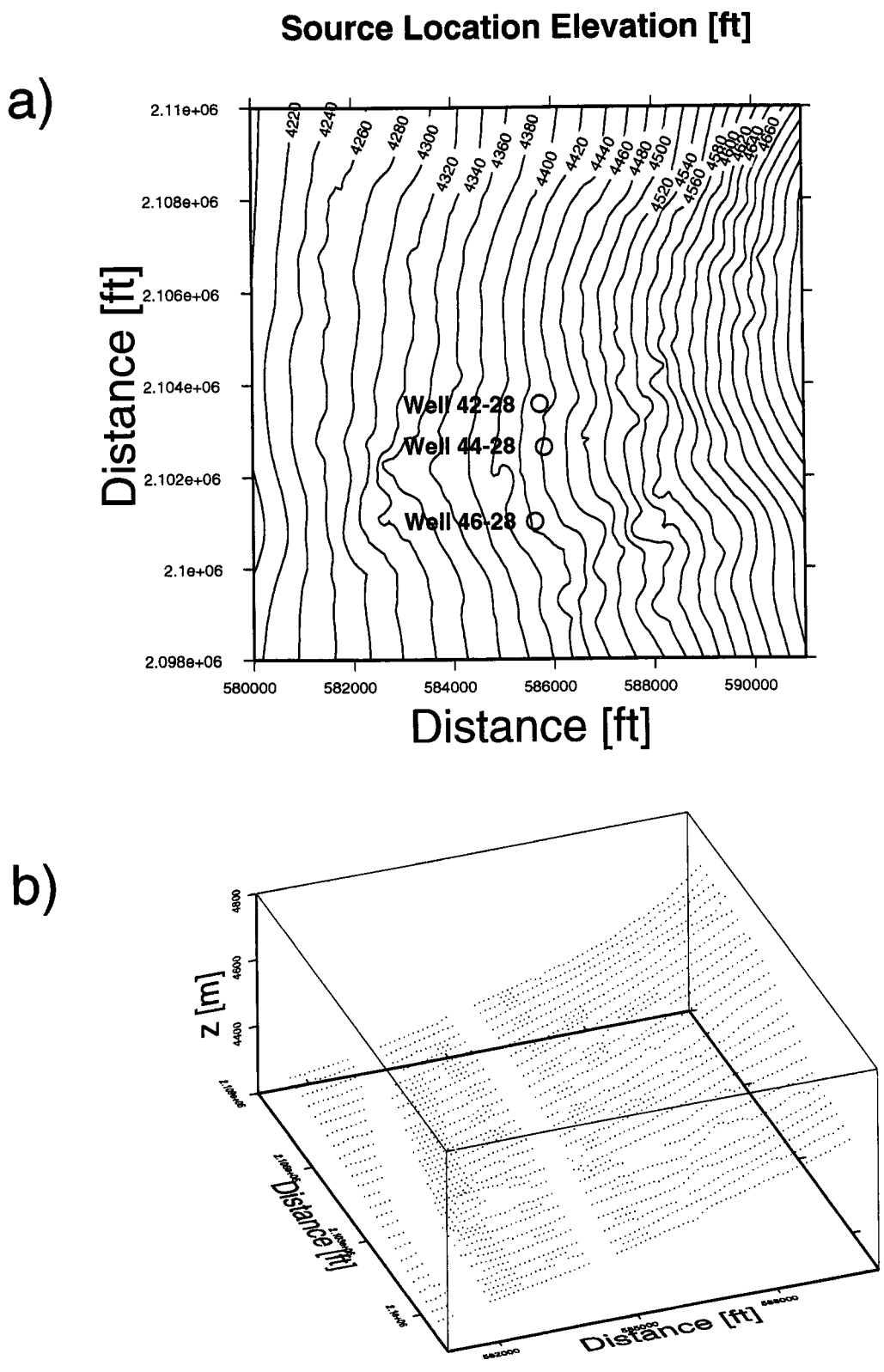

Figure 7. Map of the sources locations of the 3-D seismic surface survey. a) Contour map with well locations superimposed. b) 3-D view of individual source locations. View from South-West.

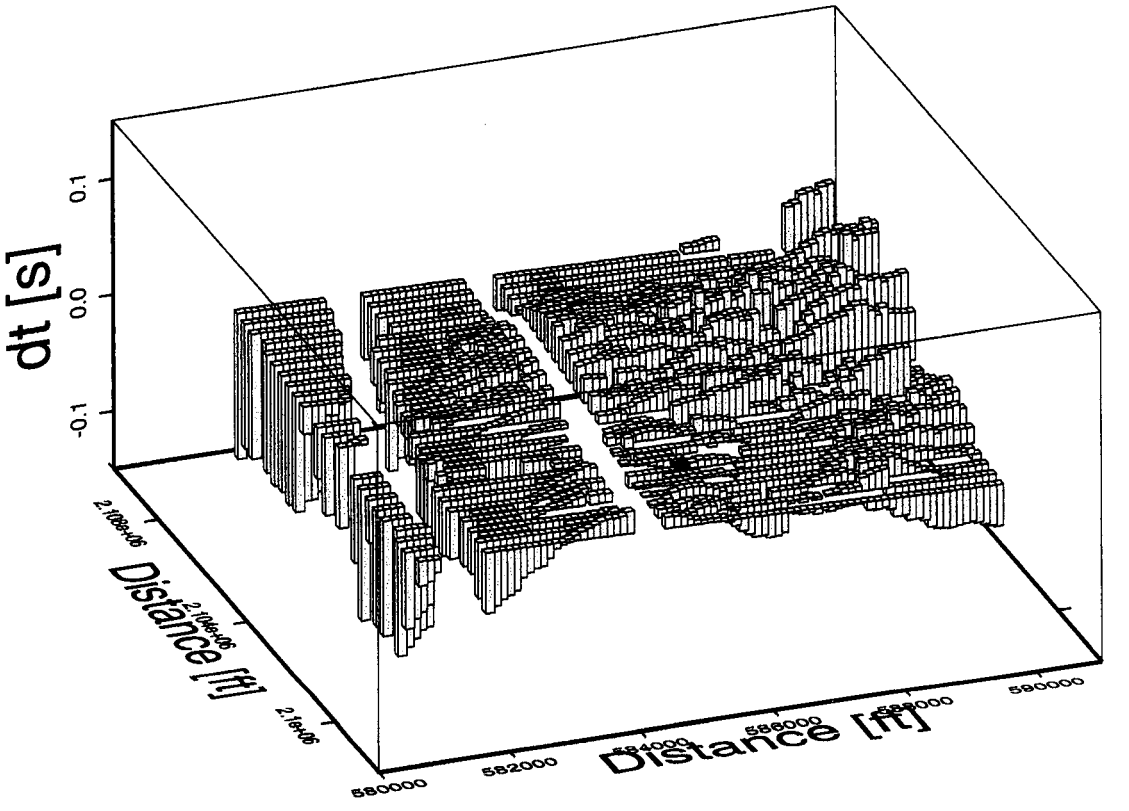

Figure 8. Travel time differences between the observed and modeled travel times, with sources located at the same elevation as the well-head of borehole 46-28. View from South-West.

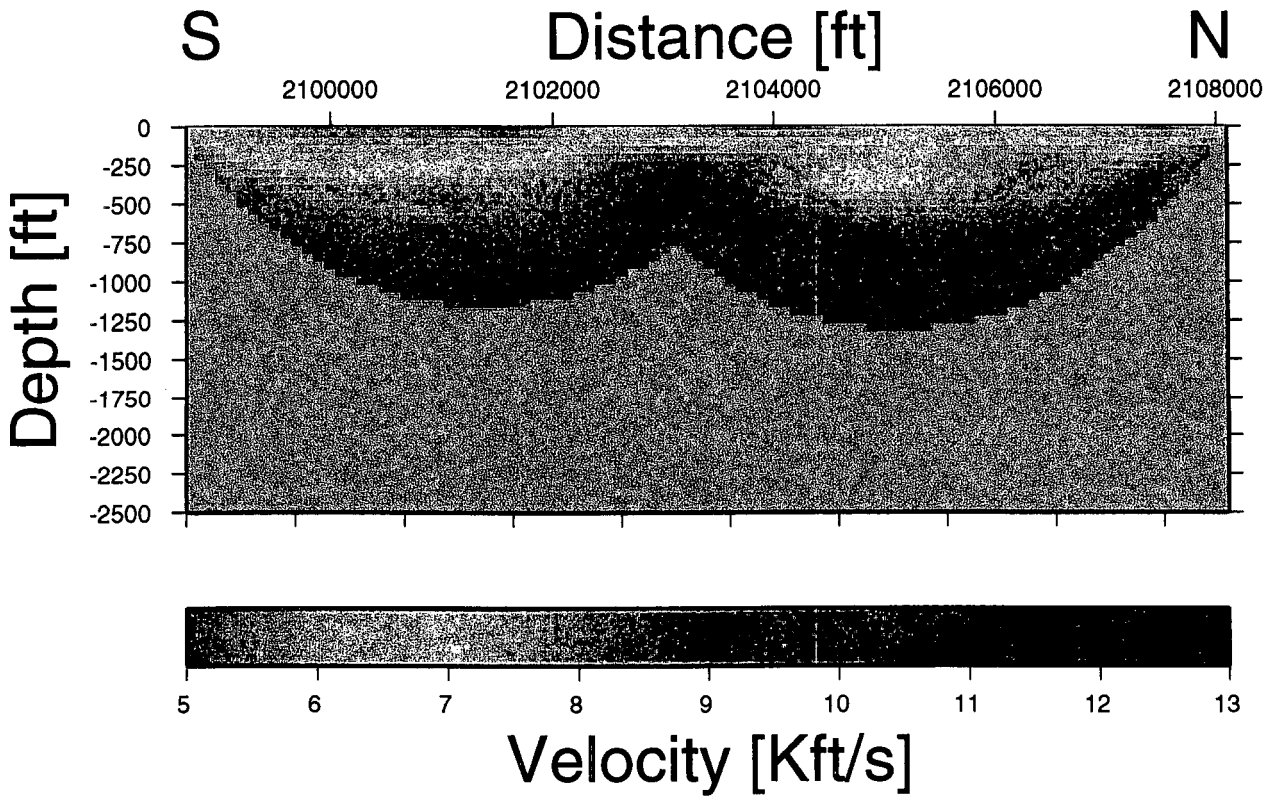

Figure 9. Velocity estimates of travel time inversion for receiver line 1 along the western boundary of the survey area.

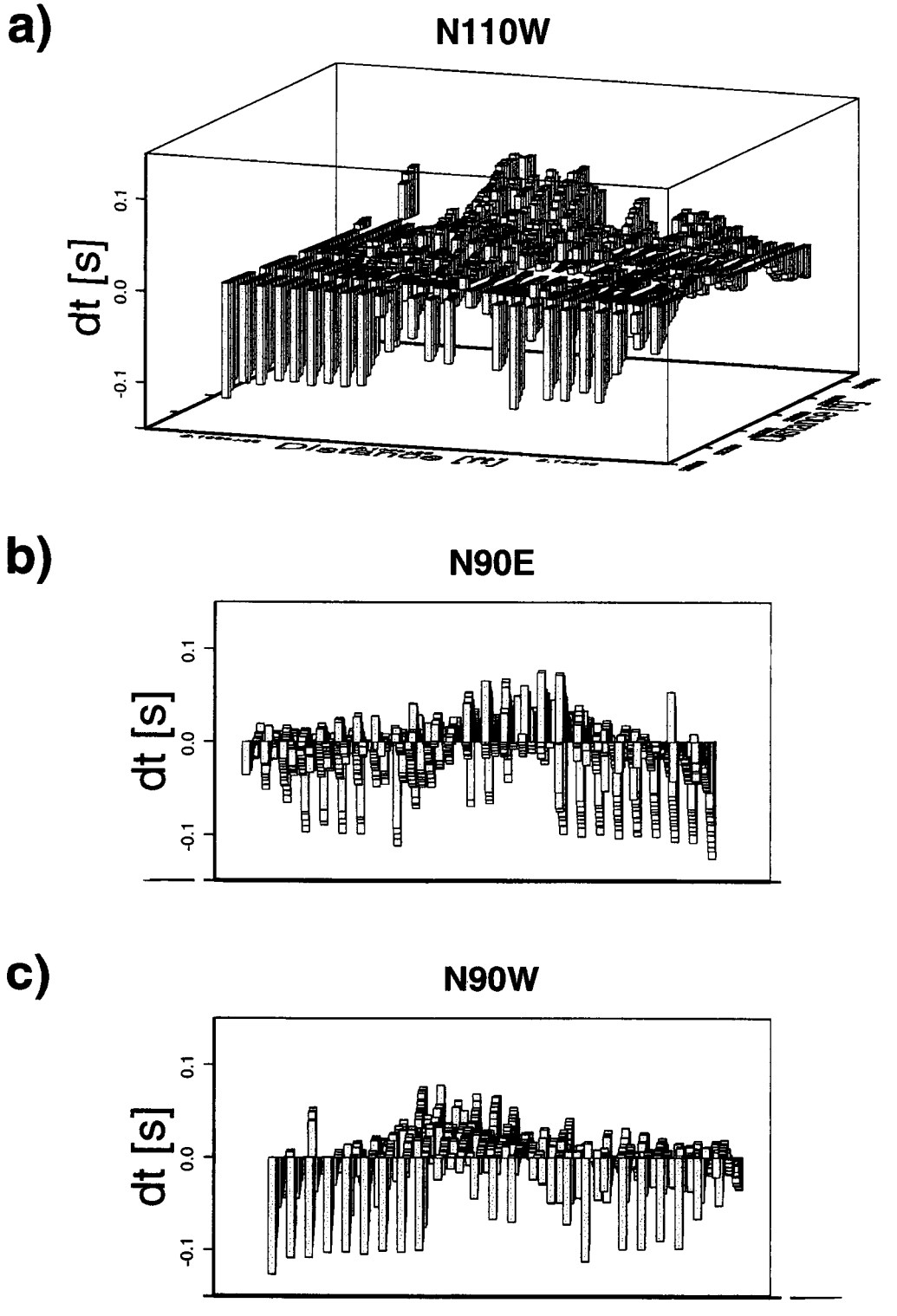

Figure 10. Travel time differences between the observed and modeled travel times view from different azimuths. a) view from South-West. b) view from East. c) view from West.

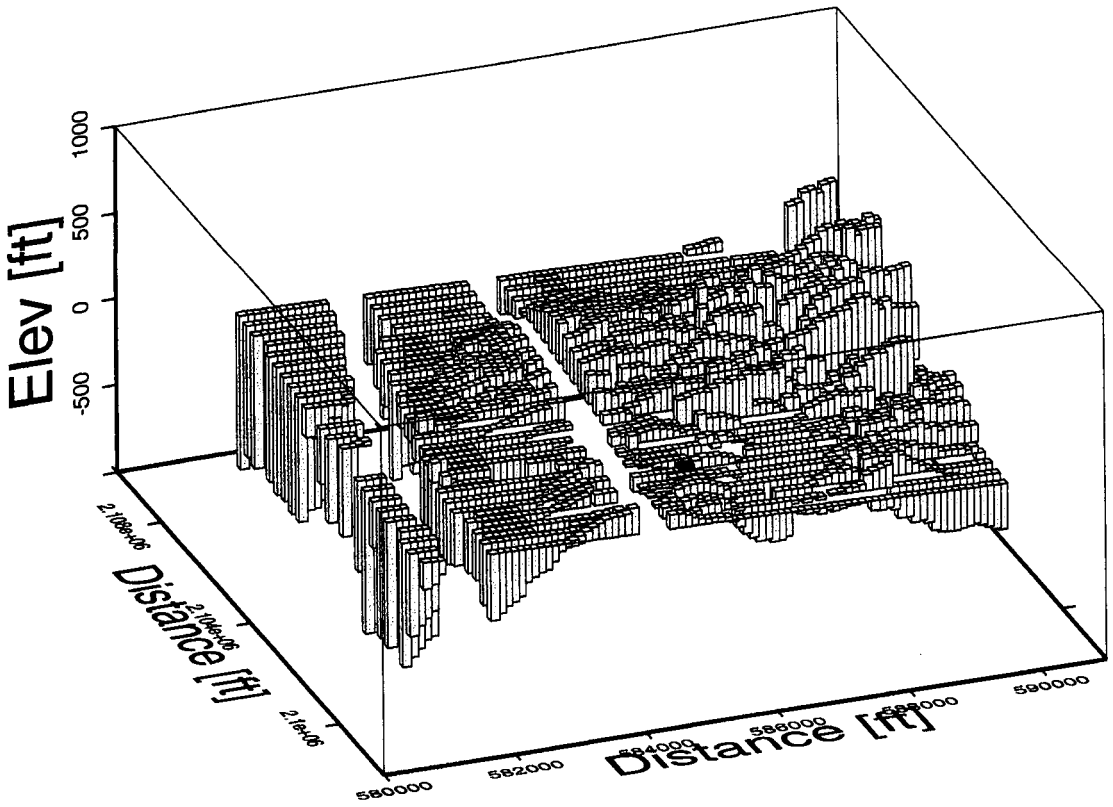

Figure 11. Variations in elevation of the basement interface. VSP well 46-28 is indicated by the circle in the foreground. View from South-West.

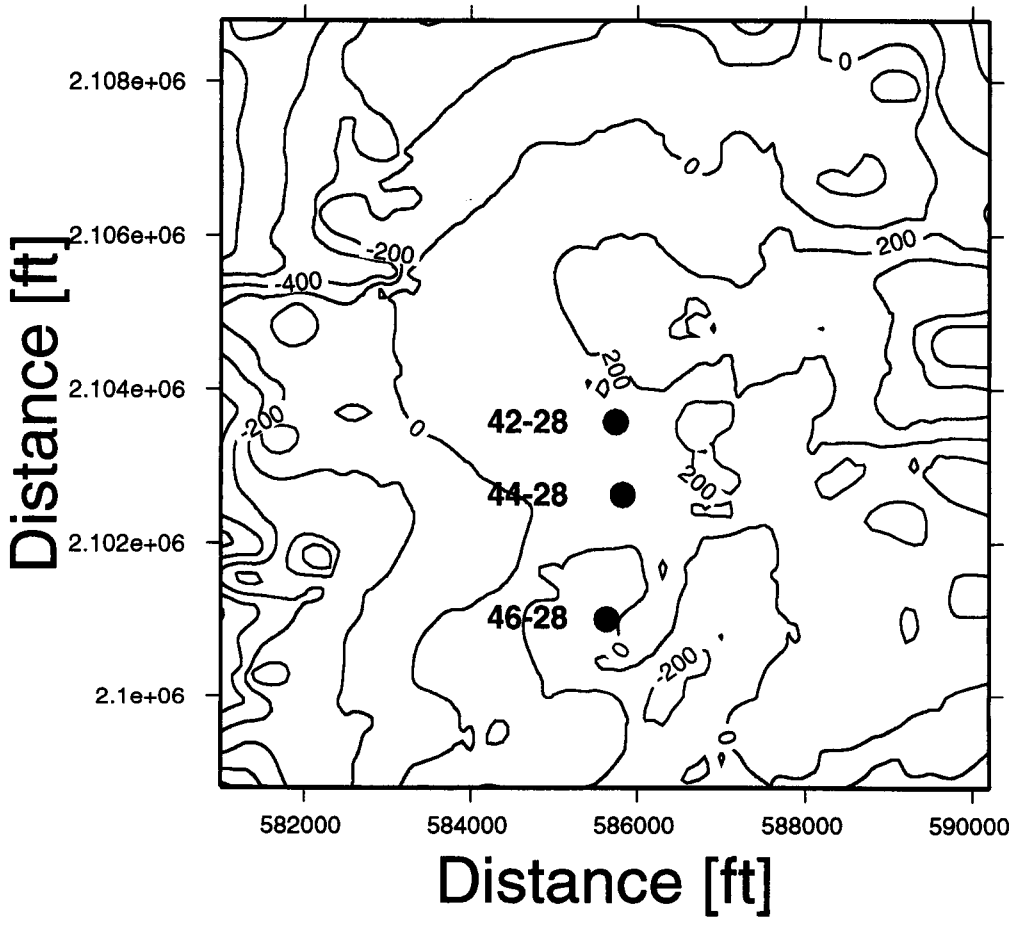

Figure 12. Contour map of the variations in elevation of the basement interface. The three boreholes are indicated for reference.

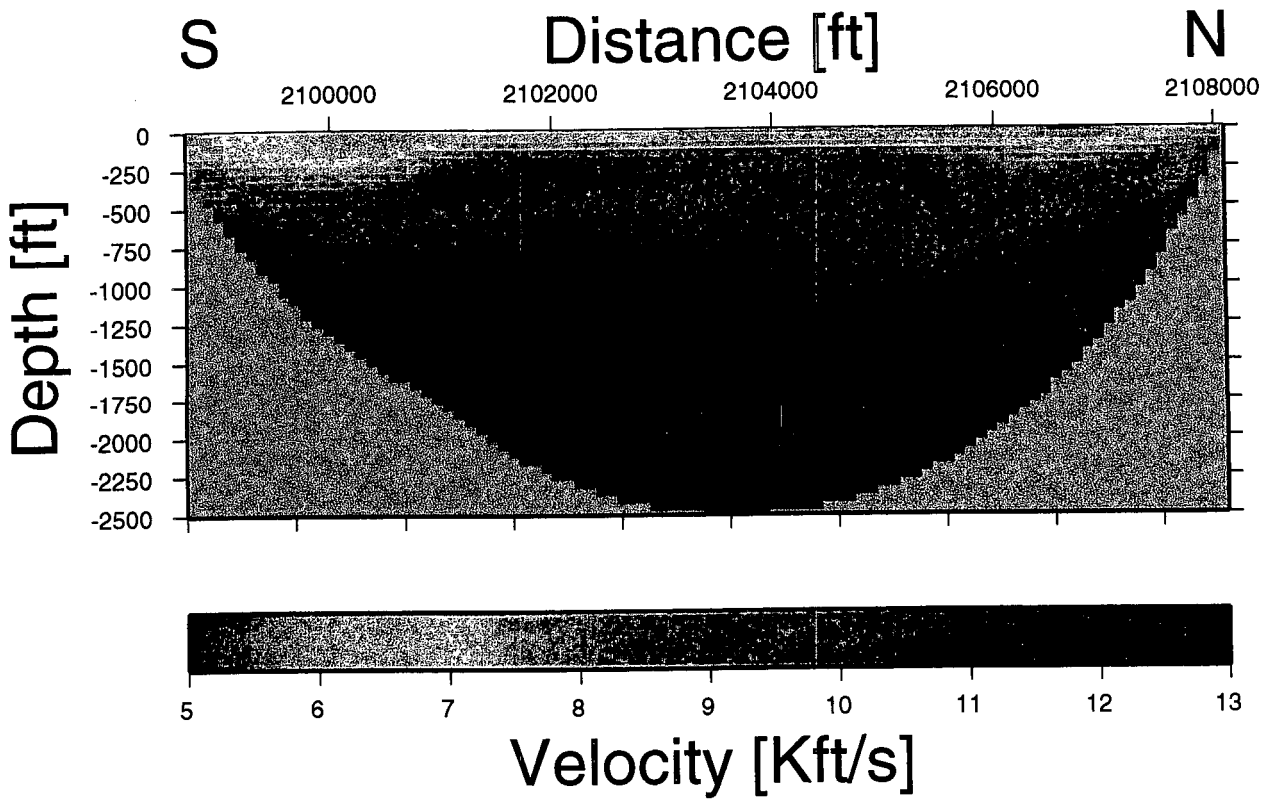

Figure 13. Velocity estimates of travel time inversion for receiver line 13 along the eastern boundary of the survey area.

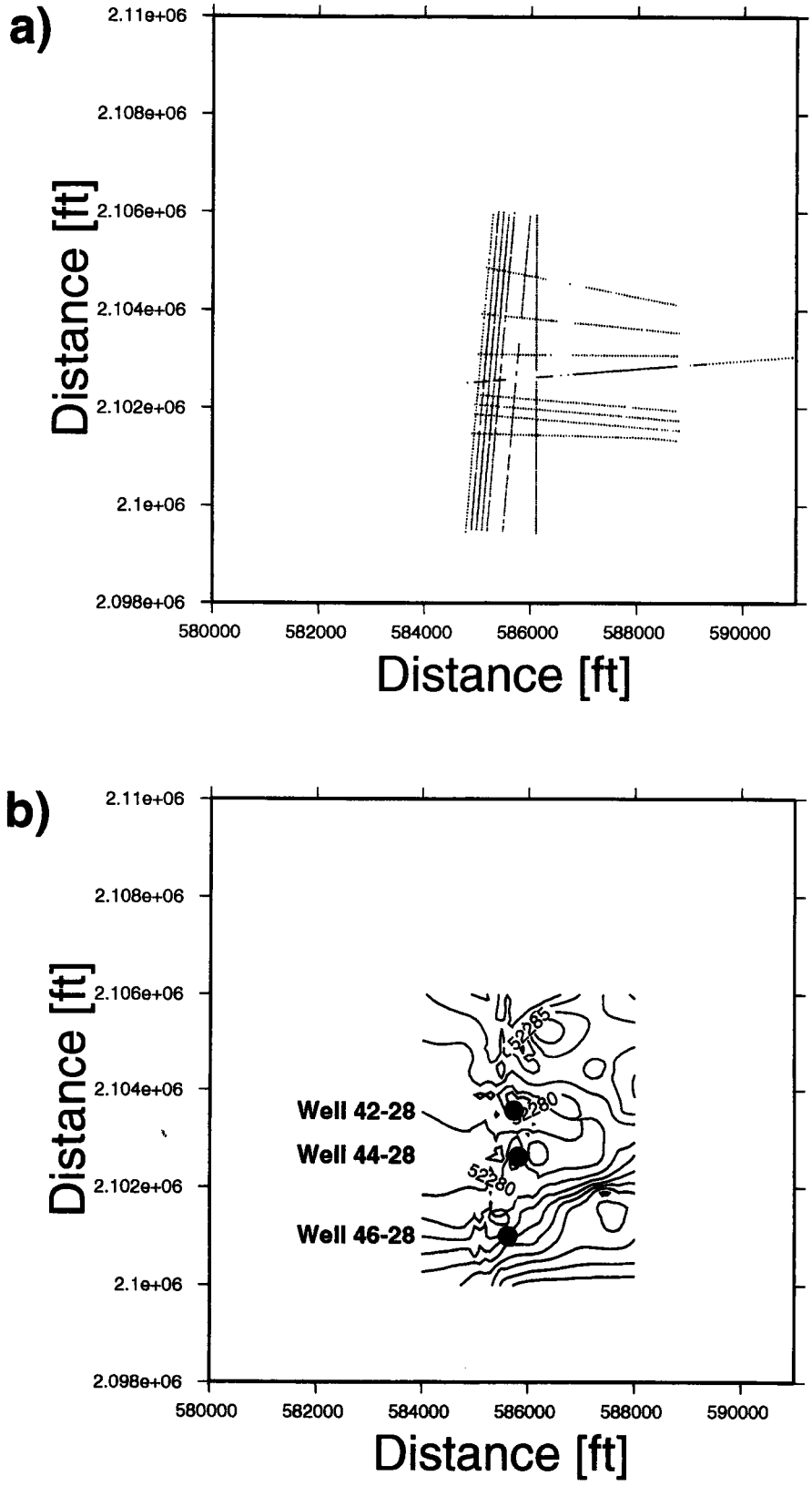

Figure 14. Results of gravity measurements at Rye Patch within the boundaries of the 3-D seismic survey area. a) Location of gravity measurements. b) Contour map of Bouguer gravity residual.

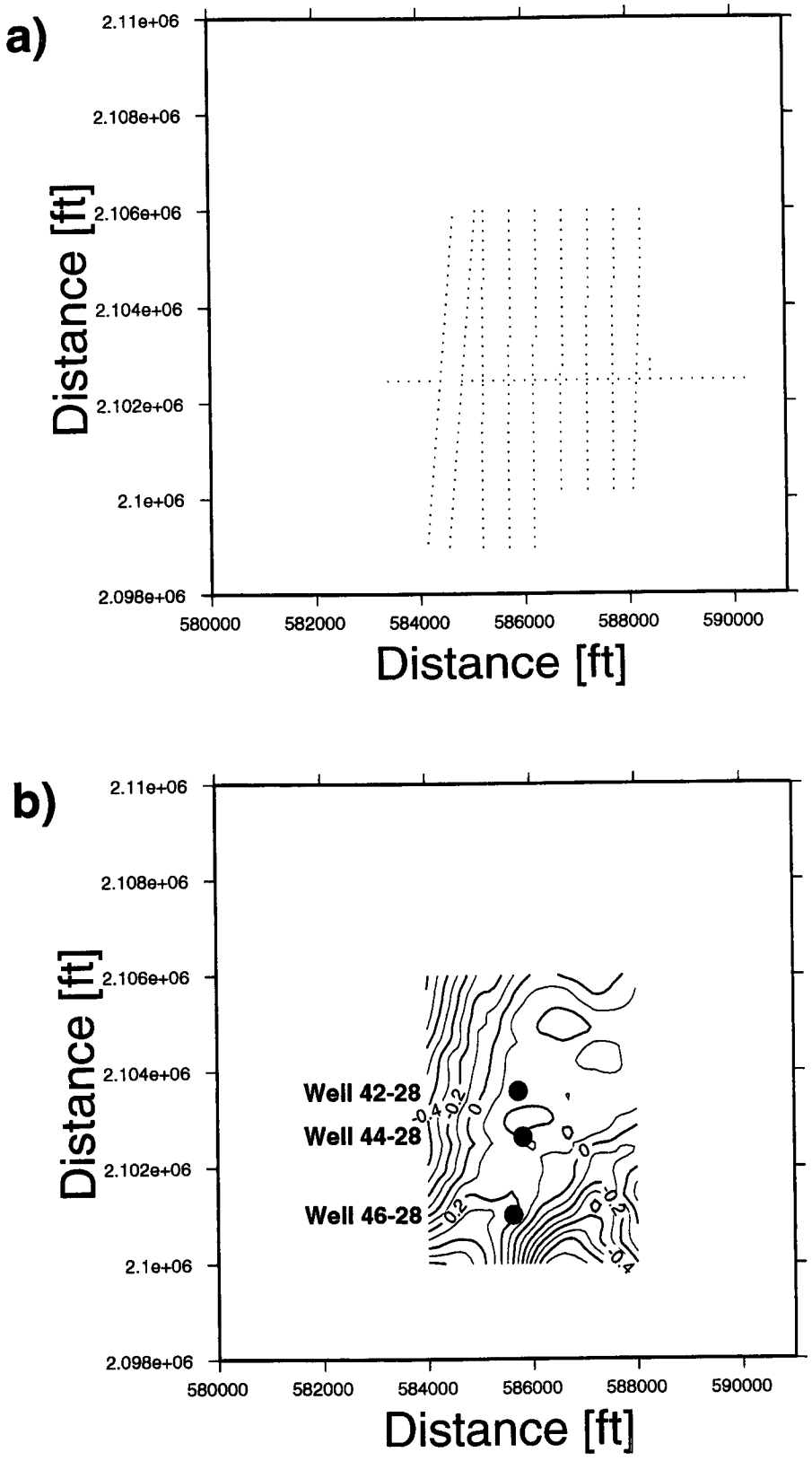

Figure 15. Results of magnetic measurements at Rye Patch within the boundaries of the 3-D seismic survey area. a) Location of magnetic measurements. b) Contour map of total magnetic field.

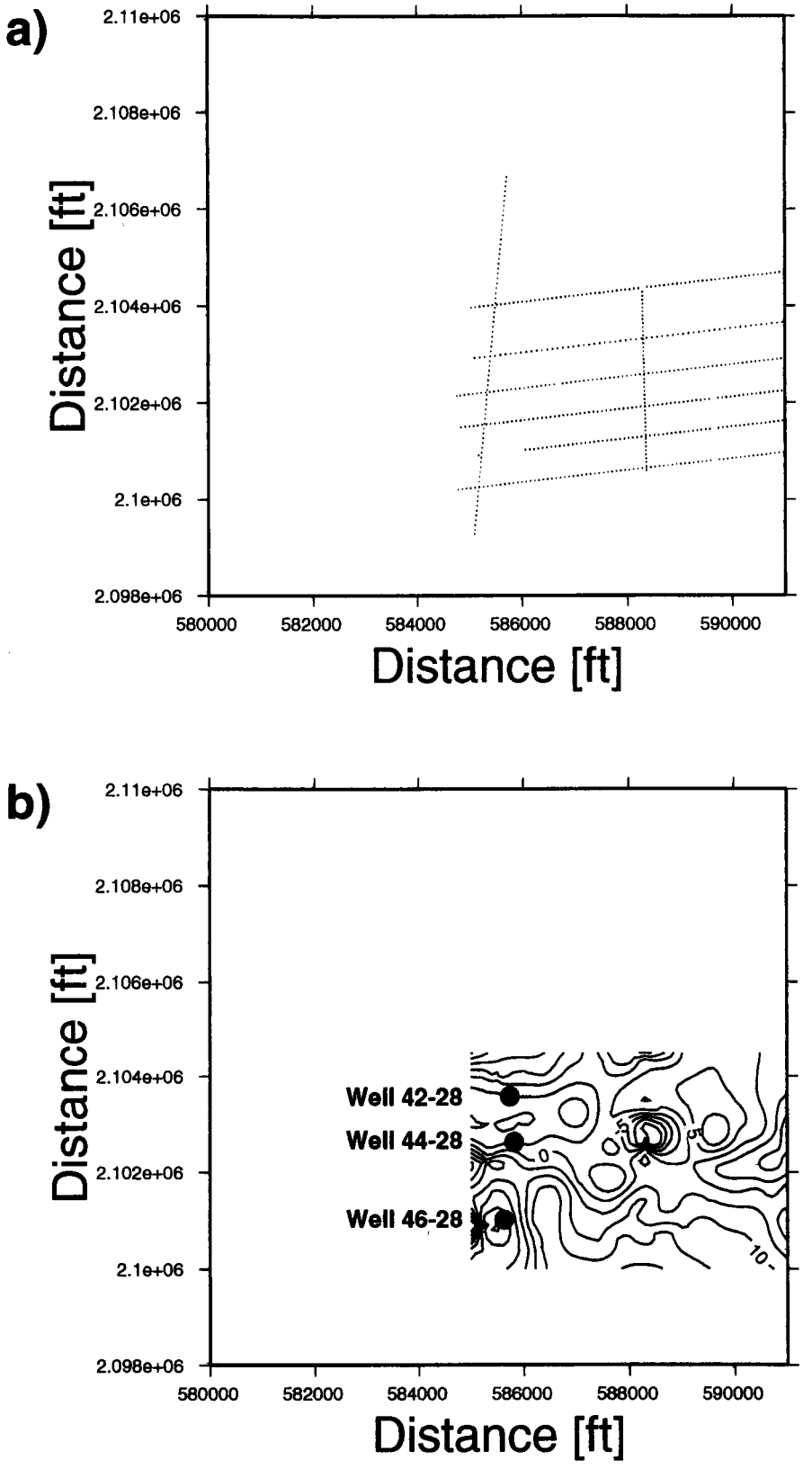

Figure 16. Results of self potential measurements at Rye Patch within the boundaries of the 3-D seismic survey area. a) Location of self potential measurements. b) Contour map of self potential field.